Materials Advances

ROYAL SOCIETY OF CHEMISTRY

PAPER

View Article Online
View Journal | View Issue

Cite this: *Mater. Adv.*, 2022, 3, 7854

Polar engineering regulates photoluminescence-tunable carbon dots for microalgal lipid imaging†

Fangmei Fu,[a] Sirui Huang,[a] Xiaoqin Pan,[a] Junjie Lin,[a] Xiaoman Huang,[a] Zishan Liang,[a] Guiling Zeng,[a] Wei Li,[ab] Haoran Zhang,[ab] Xuejie Zhang,[a] Mingtao Zheng,[ab] Yinjian Zheng,[c] Qingming Li[c] and Bingfu Lei *[a]

Received 26th June 2022,
Accepted 7th August 2022

DOI: 10.1039/d2ma00747a

rsc.li/materials-advances

At present, research on the regulation strategy and mechanism of carbon dots (CDs) fluorescence emission from short wavelength to long wavelength is a hot topic. Herein, *o*-phenylenediamine (O-PDA) was used as the sole precursor and the polarity of the reaction solvent was adjusted by changing the volume ratio of *N*,*N*-dimethylformamide (DMF) to H_2O to synthesize green (G-CDs), orange (O-CDs), and red CDs (R-CDs). All three types of CDs exhibited uniform particle sizes and excitation-independent photoluminescence (PL) emissions. The fluorescence lifetime decay curves revealed that the emission centers of G-CDs to O-CDs or R-CDs changed from double-emission centers to pure surface emission, which led to their different solvatochromic effects. X-Ray photoelectron spectroscopy (XPS), nuclear magnetic resonance spectroscopy (NMR), and mass spectroscopy (MS) techniques proved that the appropriate polarity of the reaction solvent could extend the π-conjugation of the fluorescent molecular structure on the surface of the CDs and induce a red-shift of the CDs emission. In addition, R-CDs had a relatively large nonpolar aromatic structure that showed low polarity and lipophilicity. The R-CDs dispersed in glycerol trioleate showed bright yellow fluorescence with a quantum yield (QY) of 43.52% but almost no fluorescence in water. At the same time, R-CDs had the advantages of good biocompatibility, a large Stokes shift (113 nm), and excellent photostability. Finally, as a targeted probe of microalgae lipids, R-CDs could screen the microalgae lipid-rich varieties and monitor changes in microalgae lipid content under N-free culture conditions.

Introduction

Carbon dots (CDs) are a new kind of zero-dimensional nanomaterials. The advantages of high quantum yield (QY),[1] excellent biocompatibility,[2] high photostability,[3] large Stokes shift,[4] simple synthesis,[5] low cost,[6] *etc.* have seen CDs attract extensive attention in the fields of bioimaging,[7] sensing,[8] light-emitting diodes (LEDs),[9] photocatalysis,[10] and so on. CDs with short wavelength emission are easy to be synthesized, and their QY has reached 99% to date.[11] However, short-wavelength emission CDs have no advantage in biological imaging, because the spontaneous fluorescence of biological tissues can easily interfere with them and damage tissue cells.[12] Therefore, researchers are committed to controlling the emission of CDs from short wavelength to long wavelength from the aspects of the precursors, atomic doping (N, S), reaction conditions and solvents, and have reported dramatic progress.[13–15] Among these aspects, the reaction solvent can not only provide heteroatoms, but also plays significant roles in the degree of dehydration and carbonization of the precursor.[16] Ding *et al.* found that it is easier to synthesize long-wavelength emission CDs using solvents with a lower boiling point, because solvents with a lower boiling point can generate higher vapor pressure at the same reaction temperature, thus promoting the dehydration and carbonization of the precursors.[17] Another important physical property of solvents is their polarity. The solvent polarity affects the reaction rate and the proportion of competing products in organic synthesis.[18] Similarly, in the synthesis of CDs, the polarity of the reaction solvent is also one of the important factors affecting the structure and optical properties of the CDs. Khavlyuk *et al.* synthesized onion-like CDs with phloroglucinol as the precursor and formamide (FA) as the solvent, and found that the phloroglucinol molecules in the polar FA medium tend to organize into vesicle-like structures and polymerize into onion-like structures during dehydration.[19] Aqueous solution is usually used as the main

[a] *Key Laboratory for Biobased Materials and Energy of Ministry of Education, College of Materials and Energy, South China Agricultural University, Guangzhou 510642, P. R. China. E-mail: tleibf@scau.edu.cn*
[b] *Maoming Branch, Guangdong Laboratory for Lingnan Modern Agriculture, Guangdong, Maoming 525100, P. R. China*
[c] *Institute of Urban Agriculture, Chinese Academy of Agricultural Sciences, Chengdu 610213, P. R. China*

† Electronic supplementary information (ESI) available. See DOI: https://doi.org/10.1039/d2ma00747a

reaction medium because of its safety and solubility to small molecules. However, aqueous solutions with high polarity are not conducive to the formation of conjugated PL centers, so most CDs prepared show short-wavelength emission.[20] Wang *et al.* synthesized CDs with full-color fluorescent emission (450–665 nm) by acid engineering with ethanol as the solvent, but when ethanol was replaced with formamide and water with strong polarity or toluene with weak polarity, the modulation range of the PL peak was only 450–610 nm. This proved that solvents with strong or weak polarity will lead to a blue-shift of the CDs' fluorescence.[21] In addition, the explanation of the mechanism of CDs fluorescence red-shift is not comprehensive at present. Many mechanisms to explain the red-shift of CDs have been proposed that involve improving the sp^2 hybridization of the carbon core, the graphitization degree, and the oxidation degree of the CDs' surface, without paying attention to the change in the fluorescent molecular structure on the CDs' surface. Therefore, we believe that understanding the influence of the reaction solvent polarity on the surface fluorescent molecular structure of CDs can further improve the molecular luminescence mechanism of CDs.

Microalgae with a fast growth cycle are considered a green renewable bioenergy source with great potential, mostly because they do not need cultivated land, and as their lipid content is 15 to 20 times higher than land-based oleaginous crops.[22] A quick and simple method for detecting the lipid content in microalgae can help to screen excellent lipid-rich microalgae species and optimize microalgae culture conditions. Traditional methods for determining the lipid content of microalgae, such as weighing, require large biomass and complicated extraction steps. At the same time. chromatographic methods, such as thin-layer chromatography (TLC) and high-pressure liquid chromatography (HPLC), are not suitable for the rapid analysis and real-time monitoring of microalgal lipid content due to their long detection period and high measurement cost.[23,24] Therefore, growing attention has been paid to the use of lipophilic fluorescent probes, such as Nile Red and BODIPY 505/515. However, Nile Red can also combine with other non-lipid organelles with a hydrophobic structure to emit bright fluorescence, and it does not specifically combine with lipids.[25] BODIPY 505/515 has a good and high targeting ability to lipids, but its Stokes shift is very small, which may cause self-absorption.[26] Meanwhile, the biocompatibility of fluorescent dyes is relatively poor, and the thick cell wall of microalgae usually makes it difficult for organic fluorescent dyes to permeate smoothly. In order to change the permeability of microalgae cells, organic solvents, such as DMSO, are usually used to treat microalgae cells.[27] However, the high toxicity of DMSO tends to damage microalgae cells. Therefore, there is a need to find a novel fluorescent probe with a large Stokes shift, high QY, good biocompatibility, and lipid-targeting ability for the rapid detection of microalgae lipids.

In this work, we report a novel polar engineering strategy to acquire green to red photoluminescence-tunable CDs using *o*-phenylenediamine (O-PDA) as the precursor. Detailed characterization was performed that elucidated that the red-shift of the CDs was caused by extending the π-conjugation of the fluorescent molecular structure on the surface of the CDs, which included the extended aromatic structure of fluorescent molecules and increased C═O functional groups. The electron donor (–N═C/NH_2), aromatic structure, and electron acceptor (C═O) groups on the surface of R-CDs constitute the D–π–A structure, which makes them extremely sensitive to the solvent polarity and show the characteristics of high fluorescence intensity in low polarity solvents. In addition, R-CDs have a relatively large nonpolar aromatic structure, showing low polarity and lipophilicity. Finally, R-CDs were selected as a targeted probe for microalgae lipids, and then the screening of microalgae lipid-rich varieties and the monitoring of microalgae lipid content changes in N-free culture conditions were successfully realized.

Experimental

Reagents and materials

Formamide (FA), ethylene glycol (EG), isopropanol (IPA), ethanol (EA), methanol (MA), ethyl acetate (EAC), petroleum ether (PE), dichloromethane (DCM), 1,4-dioxane, *N*,*N*-dimethylformamide (DMF), dimethyl sulfoxide (DMSO), BODIPY 505/515, and *o*-phenylenediamine (O-PDA) were purchased from Shanghai Macklin Biochemical Co, Glycerol trioleate was obtained from Shanghai Xianding Biology Science and Technology Co.

Characterization

All the characterization devices and techniques are described in the Section S1.1, ESI.†

Synthesis of the CDs

First, 0.5 g O-PDA was dissolved in 40 mL DMF, DMF/H_2O mixed solution, and deionized water respectively. The obtained solution was transferred into a 100 mL Teflon-lined stainless reactor and heated in an oven at 210 °C for 10 h. The reactor was automatically cooled to room temperature and then purified in the next step. First, the resulting mixture was purified *via* a 0.22 μm filter to remove large particles. Second, dichloromethane and water were added to the reaction products for extraction, whereby the lower organic phase layer containing the CDs was collected, while the upper aqueous solution was poured out, and the above operation was repeated three times. Then, the crude product was purified by silica gel column chromatography. The CDs with DMF and water as the reaction solvent used dichloromethane/methanol (10 : 1) mixed solution as the eluent, and the obtained pure products were named D-CDs and W-CDs, respectively. For the CDs with DMF/water (1 : 3) as the reaction solvent, pure red carbon dots (R-CDs), and orange carbon dots (O-CDs) with poor polarity were obtained by using the mixed solution of petroleum ether/ethyl acetate (5 : 2) as the eluent, and then the mixed solution of dichloromethane/methanol (10 : 1) was used as the eluent to obtain the strong polar green carbon dots (G-CDs). Finally, the eluent was removed by rotary evaporation to obtain dry CDs.

Cell culture and MTT assays

Details of the cell culture and MTT assays can be found in the ESI,† Section S1.2.

Microalgae culture

Details of the microalgae culture can be found in the ESI,† Section S1.4.

Microalgae lipid imaging

Details of the microalgae lipid imaging can be found in the ESI,† Section S1.5.

Results and discussion

Synthesis of the PL-tunable CDs

O-PDA is one of the most commonly used CD precursors, and many excellent CDs have been synthesized through it.[19] We demonstrated a one-step solvent polar engineering method for the synthesis of PL-tunable CDs by heating O-PDA in different volume ratios of DMF/H_2O mixed solvents (Fig. 1). With petroleum ether/ethyl acetate (5 : 2) as the eluent, thin-layer chromatography was preliminary used to observe the CD component in the reaction products. Under UV light (365 nm) irradiation, it was observed that the green, orange, and red fluorescent CDs were separated on the silica gel plate, and the polarity of the three kinds of CDs from green to red steadily declined (Fig. 1a). The variation of the contents of the three types of CDs showed an obvious rule: when DMF or H_2O was used as the reaction solvent, only green CDs were obtained, while orange and red fluorescent CDs were obtained when DMF and H_2O were mixed to form a mixed solution with specific polarity as the reaction solvent. When the reaction solvent was DMF/H_2O = 1 : 3, the orange and red fluorescence CD contents reached the maximum. The products synthesized with DMF (G_D-CDs), DMF/H_2O = 1 : 3 (G-CDs, O-CDs, and R-CDs), and H_2O (G_W-CDs) as reaction solvents were purified by silica gel column chromatography (Fig. 1b). The polarity and PL spectra (Fig. 1b and Fig. S1, ESI†) of the G_D-CDs, G-CDs, and G_W-CDs were similar, implying that G_D-CDs, G-CDs, and G_W-CDs belong to the same types of CDs. G-CDs, O-CDs, and R-CDs were selected for further characterization to explore the effects of mixed solvents as reaction solvents on the structure and the optical properties of the prepared CDs.

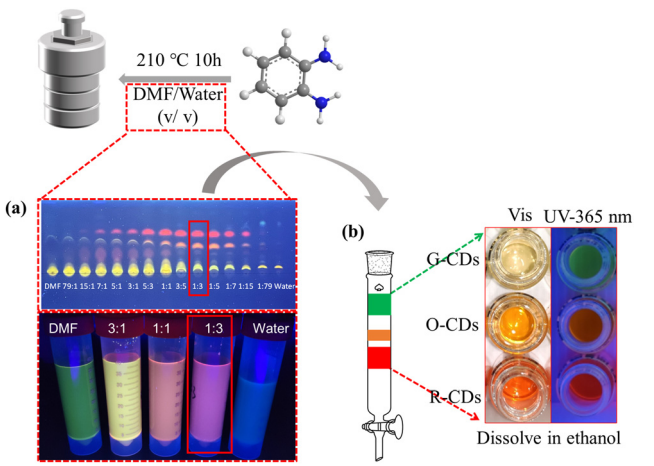

Fig. 1 Schematic diagram of the synthesis and purification of the CDs. (a) Solvent polar engineering strategy for the synthesis of PL-tunable fluorescent CDs using O-PDA as the precursor. (b) The products synthesized with DMF/H_2O = 1 : 3 (G-CDs, O-CDs, and R-CDs) as reaction solvents were purified by silica gel column chromatography.

Characterization and morphology of the CDs

As shown in Fig. 2a–c, the transmission electron microscopy (TEM) images at 50 nm resolution demonstrated that the three types of CDs were well dispersed in ethanol solution. The average diameters were determined to be 3.85, 3.38, and 3.55 nm for the G-, O-, and R-CDs, respectively (illustration at the bottom left of Fig. 2a–c), suggesting their particle size should not be responsible for their differences in fluorescence. The high-resolution TEM (HRTEM) images demonstrated that the three CDs exhibited similar well-resolved lattice fringes with a distance of 0.21 nm, which should be attributed to the (1 0 0) in-plane lattice of graphene, and indicated that the three CDs had highly crystalline carbon structures.[28]

Fourier transform infrared (FTIR) spectroscopy was performed to gain insights into the nature of the functional groups. As shown in Fig. 2d and e, the FTIR spectra of O-PDA featured $-NH_2$ vibration bands located around 3367 and 3200 cm^{-1}, respectively.[29,30] Also, the bending vibrations of the amino group were confirmed around 1591–1633 cm^{-1}, while the characteristic absorption bands at 1458–1497 cm^{-1} were attributed to benzene ring stretching vibrations. Compared with O-PDA, the three types of CDs retained the main functional groups ($-NH_2$, benzene ring) of O-PDA, indicating that a part of the groups of O-PDA may still be distributed on the CDs after the thermal process. Remarkable changes could be seen in the decrease in $-NH_2$ stretching vibrations between 3200–3300 cm^{-1} and the enhanced C–N═ stretching vibrations around 1357 cm^{-1}, which indicated that most of $-NH_2$ groups of O-PDA may be converted into the C–N═C structure during the thermal processes. In addition, the emerging stretching vibrations of –OH at 3463 cm^{-1}, C═O at 1722 cm^{-1} and C–O–C at 1198 cm^{-1} evidenced that new kinds of organic functional groups had been generated on the three types of CDs. X-Ray photoelectron spectroscopy (XPS) was employed to characterize the surface groups of the three typical CDs. The full XPS spectra of Fig. S2 (ESI†) indicated that the three CDs all contained C 1s (264.8 eV), N 1s (284.8 eV), and O 1s (532.5 eV) elements. In the exploration of the mechanism of the CDs' luminescence, the type of nitrogen is often considered the main factor in photoluminescence-tunable CDs.[31] However, the N content decreased from 7.26% to 1.58% from G-CDs to R-CDs, indicating that the red-shift of the CDs' fluorescence was not caused by N-containing functional groups. Fig. 2f–h and Table S1 (ESI†) show the high-resolution XPS spectra of the C 1s, N 1s, and O 1s elements, and the relative content of each chemical bond. The high-resolution C1s XPS spectra of the three CDs could be

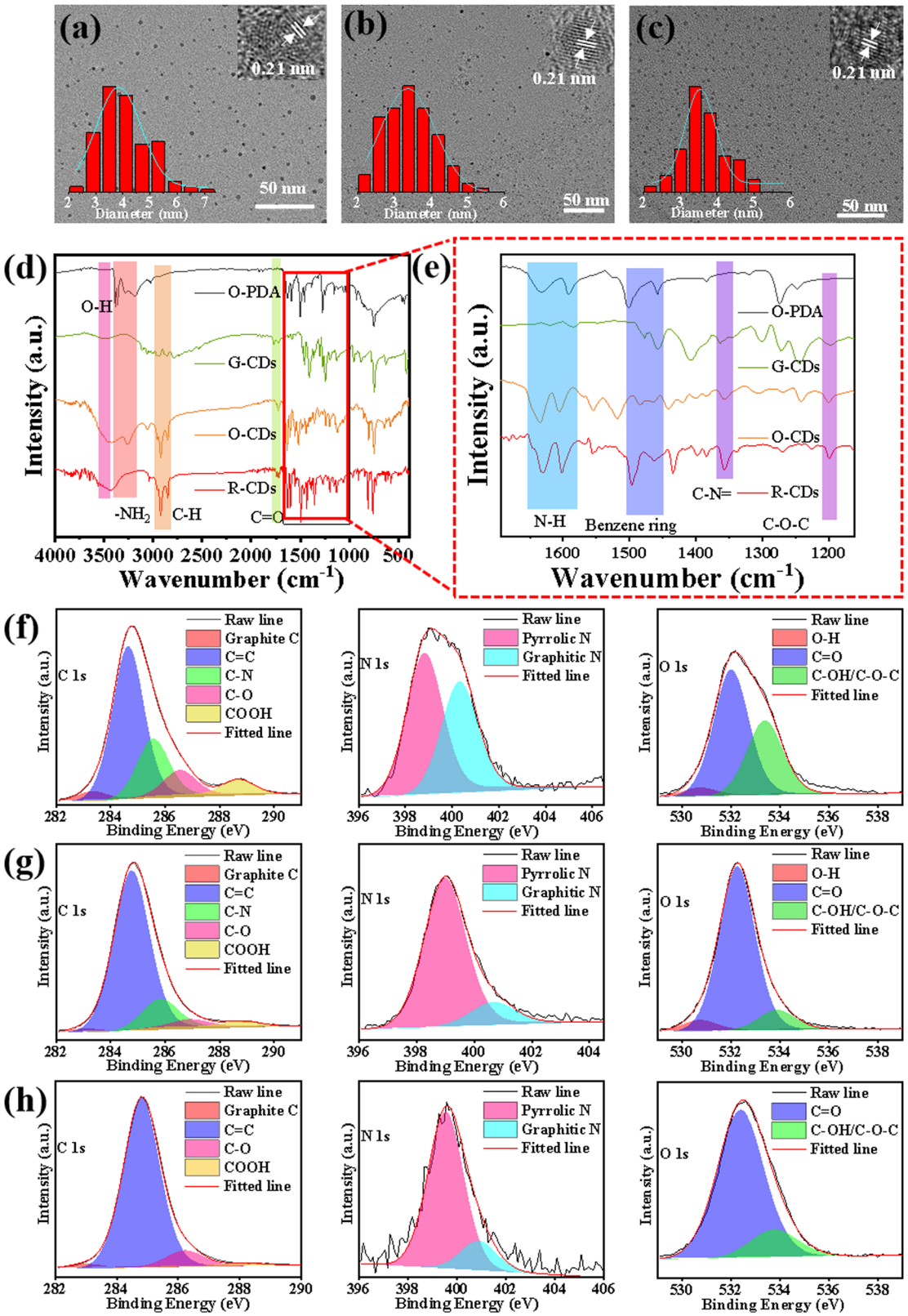

Fig. 2 Transmission electron microscopy (TEM) and corresponding diameter distribution histogram of (a) G-CDs, (b) O-CDs, and (c) R-CDs. (d) FTIR spectra and of O-PDA (black curve), G-CDs green curve), O-CDs (orange curve), and R-CDs (red curve); (e) enlarged view of (d). High-resolution XPS C 1s, N 1s, and O 1s spectra of (f) G-CDs, (g) O-CDs, and (h) R-CDs.

resolved into 5 kinds of C species: graphite C (283.0 eV), C═C (284.8 eV), C–N (285.6 eV), C–O (286.5 eV), COOH (288.6 eV). Notably, the C–C/C═C content in the R-CDs (88.2%) and O-CDs (88.8%) were significantly higher than that of the G-CDs (62.7%). From G-CD to R-CD, the content of COOH decreased from 5.7% to 1.3%, corresponding to the polarity of the three CDs gradually decreasing from G-CDs to R-CDs, which was caused by the decrease in the surface polar group –COOH and the increase in the nonpolar sp^2 conjugated structure. The high-resolution N 1s spectra of G-CDs and R-CDs could be fitted into two different types of N species: pyrrolic N and graphitic N. O-CDs also had pyridinic N on this basis. The O 1s spectra showed three peaks at 530.7, 532.0, and 533.5 eV, which were assigned to O–H, C═O, and C–OH/C–O–C, respectively. Among these, the C═O content of the R-CDs (84.7%) was much higher than that of the O-CDs (64.0%), indicating that the greater C═O content may be the reason for the further red-shift of the fluorescence.

The chemical structures of the CDs were further characterized by ^{1}H NMR and ^{13}C NMR measurements in DMSO-d6 (Fig. 3). In general, the peaks of the ^{1}H-NMR and ^{13}C-NMR spectra in the range of 6.5–8.5 ppm and 100–160 ppm represented H and C on the aromatic structures, respectively.[14] Besides, the ^{1}H-NMR and ^{13}C-NMR spectra in the range of 1–6 and 0–60 ppm were assigned to H and C in the sp^2/sp^3 hybrid structure, respectively.[32] As shown in Fig. 3a and b, the surface fluorescent molecular structure of the G-CDs was a simple aromatic compound, and there were four types of H (12.43, 8.26, 7.63–7.60, and 7.18 ppm) and C (142.43, 138.58, 112.21, and 115.80 ppm) in the aromatic structure, which was consistent with the reported ^{1}H-NMR and ^{13}C-NMR spectra of benzimidazole.[33] Liquid chromatography tandem mass spectroscopy (MS) was then applied, and the main molecular fraction a mass of m/z = 119.5 was observed for the G-CDs (Fig. S3a, ESI†), which corresponded to the mass of benzimidazole ($C_7H_6N_2$, m/z = 118.14). As shown in the ^{1}H-NMR and ^{13}C-NMR spectra (Fig. 3c–f), compared with G-CDs, the peaks at 6.5–8.5 ppm and 100–160 ppm of the O-CDs and R-CDs were obviously increased, indicating that the surface fluorescent molecular structures of the O-CDs and R-CDs had more types of sp^2 hybrid C and H. The MS (Fig. S3b and c, ESI†) showed that main molecular fractions with a mass of m/z = 210.2 and m/z = 224.4 for the O-CDs and R-CDs, respectively, which were obviously larger than the molecular weight of the G-CDs. XPS also proved that the content of C–C/C═C increased gradually from G-CDs to O-CDs or R-CDs, indicating that the increase in molecular weight was caused by the increase in the sp^2 conjugated structure.

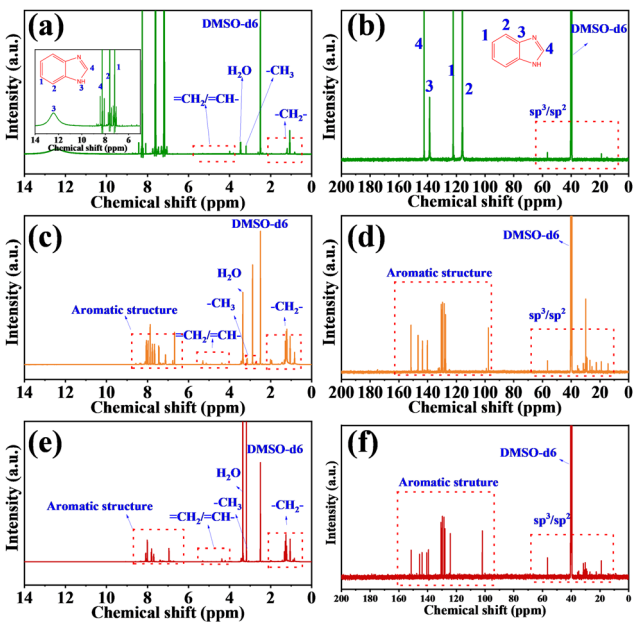

Fig. 3 ^{1}H-NMR spectra of (a) G-CDs, (b) O-CDs, and (c) R-CDs recorded in DMSO-d_6. ^{13}C-NMR spectra of (d) G-CDs, (e) O-CDs, and (f) R-CDs recorded in DMSO-d_6.

Optical properties of the CDs

Optical properties of three types of CDs were thoroughly investigated. As shown in Fig. 4a–c, the optimal PL excitation peaks were located at 379 nm for G-CDs, 478 nm for O-CDs, and 487 nm for R-CDs. The fluorescent spectra of the G-CDs, O-CDs, and R-CDs featured an excitation-independent behavior with peaks at 544, 591, and 620 nm showing green, orange, and red (Fig. 4i), respectively. The excitation-independent behavior of the CDs is similar to that of traditional organic dyes, implying that the fluorescence of CDs originates from fluorescent molecules. It is worth noting that the fluorescent molecular groups did not exist independently, but were attached or connected to the surface of the CDs. Even though the same fluorescent molecules existed on different CDs, with different synthesis conditions, the fluorescent properties and physical and chemical properties between the CDs were different, caused by the synergistic effect of the carbon core, other surface functional groups, and fluorescent molecules.[34–36] The results of the FTIR and XPS spectra show that the G-CDs, O-CDs, and R-CDs formed D–π–A structures, which were composed of –OH, C–N═/–NH_2 as electron donors, C═O as electron acceptors, and sp^2 conjugate structure as π-spacers. When the CDs were dispersed in different organic solvents, intramolecular charge transfer (ICT) may occur between the electron donor and the electron acceptor, leading to the fluorescence of the three CDs being affected by different solvent environments. As shown in Fig. 4d–f and Fig. S4 (ESI†), the fluorescence of the three CDs dispersed in organic solvents with different polarities did change. The emission of O-CDs and R-CDs was red-shifted 123 nm and 160 nm, respectively, from petroleum ether with a nonpolar nature to water with a polar nature, while that of G-CDs was only shifted 56 nm, indicating that the G-CDs were much less sensitive to the solvent polarity than the O-CDs and R-CDs. Unlike the emission spectra, the solvent-dependent shifts of the absorption spectra of the three CDs were smaller (Fig. S5a–c, ESI†), because the ground state of fluorescence was less polar than the excited state, and so the ground state was less influenced by solvents.[37] Table S2 (ESI†) collates the Stokes shifts of the three CDs in different solvents and the polarity parameter $E_T(30)$ of the solvents. Fig. S6 (ESI†) shows there was

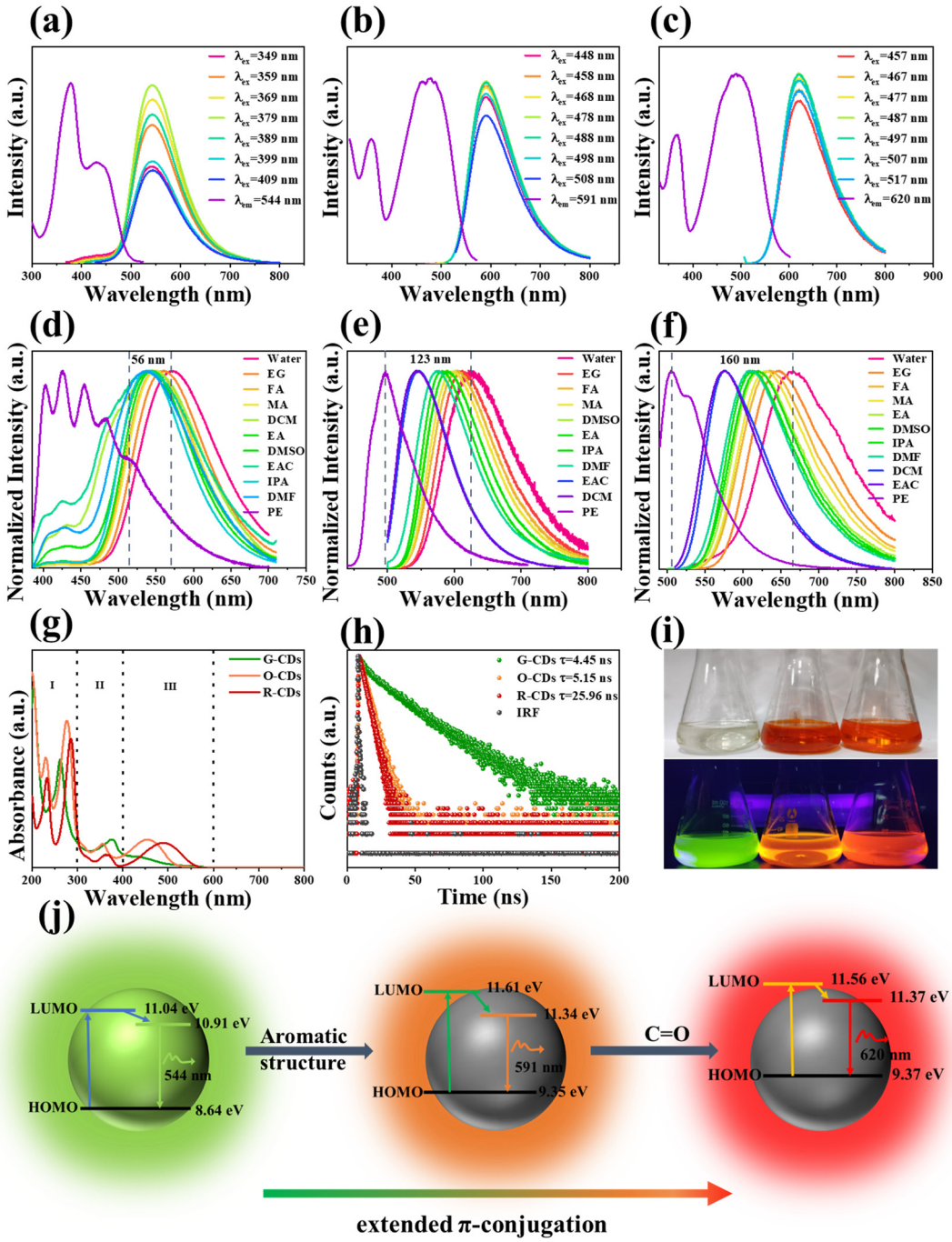

Fig. 4 (a–c) PL excitation spectra and PL emission spectra under different excitation of G-CDs, O-CDs, and R-CDs in ethanol. (d–f) PL emission spectra in different solvents of G-CDs (λ_{ex} = 379 nm), O-CDs (λ_{ex} = 478 nm), and R-CDs (λ_{ex} = 487 nm). (g) UV-vis absorption of G-CDs, O-CDs, and R-CDs in ethanol. (h) Time-resolved PL spectra of the three types of CDs. (i) Photographs of the three types of CD ethanol solutions taken in daylight (up) and 365 nm excitation (down). (j) Schematic diagram of the structure and energy level changes of the G-CDs, O-CDs, and R-CDs.

a certain linear relationship between the Stokes shifts of the G-CDs, O-CDs, and R-CDs in different solvents and the polarity parameter $E_T(30)$, and the correlation coefficients (R) were 0.855, 0.942, and 0.939, respectively. Here, the R and slopes of the linear equation fitted by G-CD were smaller than for the O-CDs and R-CDs, which proved that the G-CDs had a weak response to the polarity of the solvents. In order to further explore the difference between the G-CDs and O-CDs or R-CDs, a binary solvent system consisting of a strong polar solvent water and weak polar solvent, *i.e.*, 1,4-dioxane, was selected. By changing the volume percentage of water in the system to simulate the change in solvent polarity. Fig. S7a–f (ESI†) show that the emission peak or fluorescence intensity of the O-CDs and R-CDs and solvent polarity (Δf = 0.021–0.321) had a good linear relationship. With the increase in polarity of the binary solvent system, the fluorescence intensity of the O-CDs and

R-CDs decreased and the emission peak was red-shifted, which indicated a typical intramolecular charge-transfer (ICT) phenomenon.[38,39] However, although the emission peak position of the G-CDs was shifted to red with the increase in polarity (Fig. S7g and h, ESI†), the fluorescence intensity showed a trend of first increasing and then decreasing (Fig. S7g and i, ESI†). The reason for this phenomenon is that G-CDs have strong polarity and low solubility in 1,4-dioxane solvent with poor polarity. By adding water into 1,4-dioxane solvent, the binary solvent will form hydrogen bonds with the G-CDs, which will increase the solubility of the G-CDs in the system and lead to the increase in fluorescence intensity. As the polarity of binary solvent system continues to increase, this also further increases the hydrogen bonds, which improves the efficiency of the internal conversion and leads to vibration relaxation of the excited state of the G-CDs. Because of the internal conversion, vibration relaxation and radiation transition back to the ground state are competitive, and the increase in efficiency of the former two will lead to the decrease in photons emitted by radiation transition, and so the fluorescence intensity will decrease.[40] This shows that hydrogen bonding affects the fluorescence intensity of G-CDs by affecting the solubility and photophysical process of G-CDs. As shown in the Fig. 4g, the UV-vis absorption spectra of the three CDs were divided into three regions: 200–300 nm (region I), 300–400 nm (region II), and 400–600 nm (region III). The absorption peaks in region I and region II were attributed to the π–π* transition of the aromatic C=C bond and the n–π* transition from the sp^2 system containing C=N/C=O, respectively.[41,42] The absorption peaks in region III in the visible-light band were attributed to the n–π* transition of C=O at the edge of the sp^2 conjugate domain.[43] In Fig. 4h, the decay curves of the O-CDs and R-CDs could be fitted by a single exponential function and the fluorescence decay lifetimes were 5.15 ns and 4.27 ns, respectively. CDs with a core state and defect state emission are generally insensitive to solvents, while CDs with molecular state emission are more easily affected by the solvent polarity and hydrogen bonds.[44] The significant solvent effect and decay curves of the O-CDs and R-CDs indicated that their fluorescence came from the single emission center of the surface fluorescent molecule. The decay curve of G-CDs could be fitted to two exponentials. The short lifetime component (τ_1) and long lifetime component (τ_2) correspond to the radiative transition process of the core state and molecular state, respectively,[45,46] which indicated that the G-CDs have two emission centers originating from the core state and molecular state. The lifetime decay curves of G-CDs in different solvents were all fitted by two exponents (Table S3, ESI†). According to the different solvent properties, the contribution ratios of τ_1 and τ_2 were obviously different, whereby the contribution ratio of τ_2 was large in protic solvents, while τ_1 was dominant in aprotic solvents. Table S2 (ESI†) show that the emission peaks of G-CDs in 4 aprotic solvents were very close (DMSO 541 nm, DMF 535 nm, DCM 544 nm, EAC 539 nm), suggesting that when G-CDs are distributed in an aprotic solvent, the emission mainly originates from the core state. Conversely, i protic solvents, the hydrogen bond between the surface fluorescent molecular structure of the G-CDs and the solvent molecules makes the surface state become the main emission center. This reveals the reason why the G-CDs displayed a unique solvent dependence different from the O-CDs and R-CDs. The double-emission center of the G-CDs makes them more stable than in the case for the pure molecular state emissions of the O-CDs and R-CDs.

Emission mechanism and formation mechanism of the CDs

In order to reveal the changes in the energy levels structure of these three CDs, the highest occupied molecular orbital (HOMO) energy levels of CDs were determined by ultraviolet photoelectron spectroscopy (UPS). According to the data in Fig. S8(a–c G-CDs, d–f G-CDs, g–i G-CDs) (ESI†) the HOMO energy levels of the G-CDs, O-CDs, and R-CDs were calculated as 8.64, 9.15, and 9.37 eV, respectively. The band gap energy level was calculated by the equation $E_g = 1240/\lambda_{abs}$, where λ_{abs} is the maximum absorption edge (Fig. S8j, ESI†), and the calculated energy band gaps of the G-CDs, O-CDs, and R-CDs were 2.396, 2.361, and 2.188 eV, respectively. The changes in the energy levels and structures of three CDs are shown in Fig. 4j. With the red-shift of emission of the CDs, the HOMO energy level inside the CDs increased from 8.64 eV to 9.37 eV, and the band gap energy level between the HOMO and the lowest unoccupied molecular orbital (LUMO) decreased from 2.396 eV to 2.188 eV. The fluorescence lifetime results found that there were core state and molecular state emission centers in the G-CDs; whereas the O-CDs and R-CDs showed pure molecular state emission, which makes the O-CDs and R-CDs sensitive to changes in the solvent environment. The XPS, NMR, and MS results proved there was a simple fluorescent molecule (benzimidazole) on the surface of the G-CDs, while the fluorescent molecules on the surfaces of O-CDs and R-CDs had larger and more complex aromatic structures. Therefore, the red-shift from the G-CDs to O-CDs or R-CDs was caused by the narrow band gap resulting from the extended π-conjugate domain of the aromatic structure. Extending the conjugation is a typical red-shift method. The conjugation effect makes π electrons delocalize and flow in the whole conjugation system. This delocalization effect makes the orbit have a greater bonding property, thus reducing the energy and making the π electrons easily excited. At the same time, the maximum wavelength of the absorption band shifts to long wavelength and the body color is red-shifted.[47] The UV-vis absorption spectrum and color from G-CDs to R-CDs also gradually red-shifted and the HOMO–LUMO gaps were narrowed, which completely accorded with the characteristics of an extended conjugation, indicating that the appropriate polarity of the reaction solvent can promote the expansion of the conjugate domain of the fluorescent molecular structure on the surface of the CDs, thus realizing the long-wavelength emission of the CDs. The physical properties (polarity, solvent effect, UV-vis absorption spectrum, and lifetime) of the O-CDs and R-CDs were similar, indicating that their structures were only slightly different. The NMR peaks at 6.5–8.5 ppm and 100–160 ppm of

the O-CDs and R-CDs were similar, while the molecular weight of the R-CDs (m/z = 224.4) detected by MS differed from that of the O-CDs (m/z = 210.2) by only 14, and the high-resolution C 1s spectra of the O-CDs (88.8%) and R-CDs (88.2%) showed that their C–C/C=C contents were approximately the same. These data demonstrate that the difference between them was not in their aromatic structure. The high-resolution O 1s spectra showed that the content of C=O in the R-CDs (84.7%) was obviously higher than that of the O-CDs (64.0%), indicating that the red-shift from O-CDs to R-CDs may be caused by the presence of a greater content of C=O in the R-CDs. In the design of organic fluorescent molecules, it has been reported that C=O can improve the conjugation degree of the whole system, resulting in a red-shift of the fluorescence,[48,49] which is consistent with our research results.

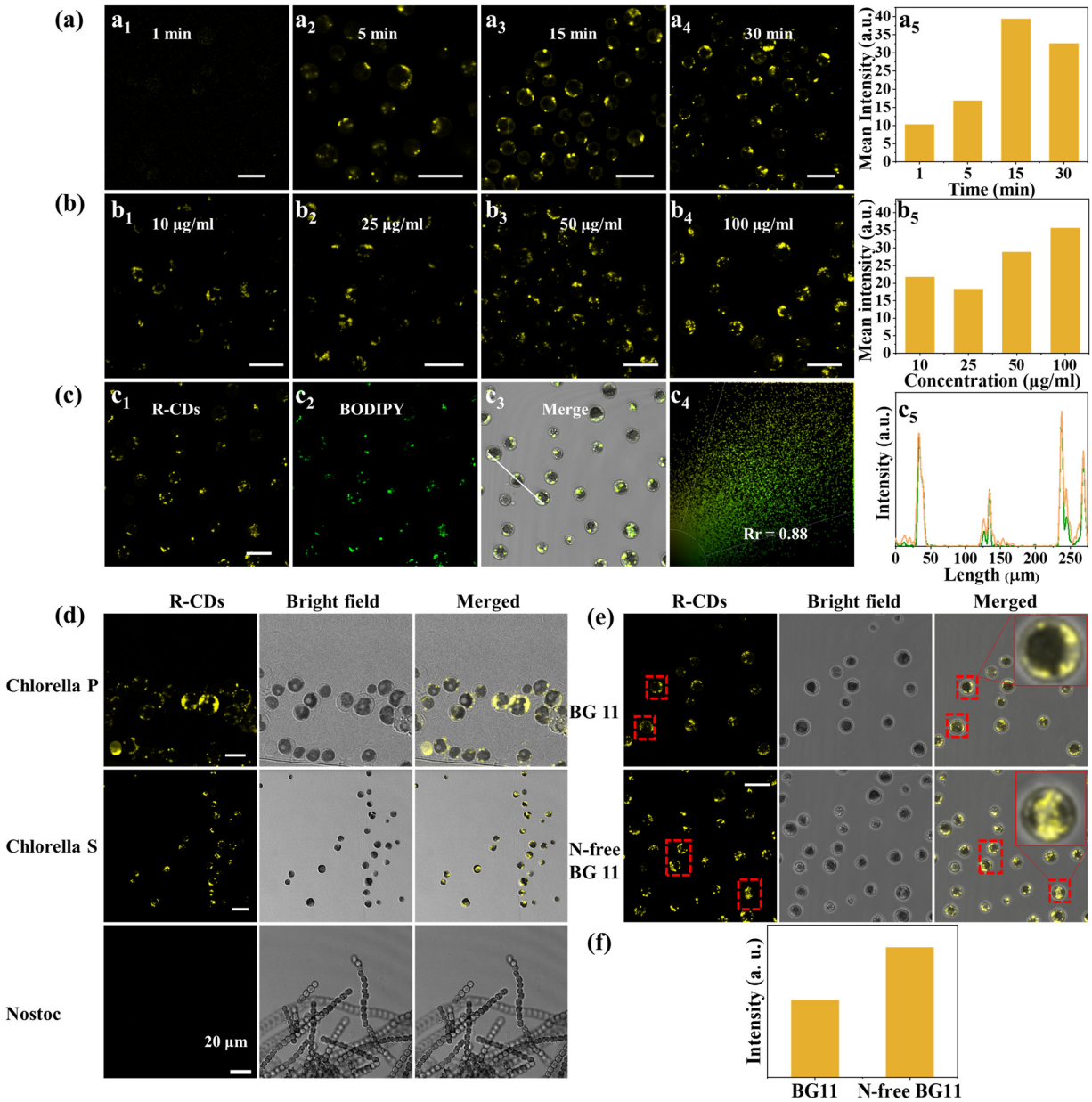

Fig. 5 (a) (a_1–a_4) Confocal images of *Chlorella S.* treated with 50 μg mL^{-1} R-CDs (λ_{ex} = 488 nm, λ_{em} = 560–625 nm) for different times (0–30 min). (a_5) Mean fluorescence intensity of (a_1–a_4.); (b) (b_1–b_4) images of *Chlorella S.* treated with different concentrations (10–100 μg mL^{-1}) R-CDs for 15 min. (b_5) Mean fluorescence intensity of b_1–b_4.; (c) colocalization images of *Chlorella S.* incubated with 50 μg mL^{-1} R-CDs and 4 μg mL^{-1} BODIPY 505/515 for 15 min. (c_1) Yellow fluorescence of R-CDs (λ_{ex} = 405 nm, λ_{em} = 577–625 nm). (c_2) Green fluorescence of BODIPY 505/515 (λ_{ex} = 488 nm, λ_{em} = 500–641 nm). (c_3) Merged. (c_4) Correlation plots of BODIPY 505/515 targeting probes and R-CDs. (c_5) Curve of fluorescence intensity between the green and yellow channels in *Chlorella S.*; scale bar: 10 μm. (d) Confocal images of *Chlorella P.* (scale bar: 10 μm), *Chlorella S.* (scale bar: 10 μm) and *Nostoc.* (scale bar: 20 μm), treated with 50 μg mL^{-1} R-CDs (λ_{ex} = 488 nm, λ_{em} = 560–625 nm) for 15 min; (e) confocal images of *Chlorella S.* cultured in BG11 and N-free BG11, treated with 50 μg mL^{-1} R-CDs for 15 min. Scale bar: 20 μm; (f) mean fluorescence intensity of *Chlorella S.* cultured in BG11 and N-free BG11.

Microalgae lipid imaging

As mentioned above, among the three CDs, R-CDs had a relatively large nonpolar aromatic structure, showing low polarity and lipophilicity. Based on these characteristics, the R-CDs were selected as a fluorescent probe for lipids in microalgae. The QY of the R-CDs dispersed in glycerol trioleate was 43.52%, whereas there was almost no fluorescence in water. From this base, a favorable signal-to-noise ratio can be achieved in microalgae lipid imaging. The optimal excitation and emission of R-CDs dispersed in glycerol trioleate were 462 nm and 575 nm (Fig. S9, ESI†), respectively, and the Stokes shift reached 113 nm, avoiding self-absorption. The cytotoxicity of R-CDs in HeLa cells was evaluated by MTT assay. Fig. S10 (ESI†) shows that even when the concentration was as high as 100 μg mL^{-1}, the cell survival rate was still 100%, which showed that the R-CDs have the advantages of low toxicity and excellent biocompatibility. R-CDs and BODIPY 505/515 were dispersed in glyceryl trioleate, and the fluorescence intensity of BODIPY 505/515 was found to be decreased by 20% while that of R-CDs was only decreased by 5% after irradiation with a blue lamp (405 nm) with a power of 6 W for 30 min (Fig. S11, ESI†), which indicated that the R-CDs had better photostability. Because the cell wall of microalgae is thick, R-CDs take longer to enter the microalgae cells than animal cells. Exploring the best treatment time can allow accurately imaging lipids in microalgae. As shown in Fig. $5a_{1-5}$, *Chlorella S.* was treated with R-CDs and obvious fluorescence signals could be observed as soon as 5 min, and the average fluorescence intensity in *Chlorella S.* reached the highest at 15 min treatment. The concentration of R-CDs is also a key factor that affects the imaging quality. Fig. $5b_{1-5}$ shows that both 50 μg mL^{-1} and 100 μg mL^{-1} R-CDs showed a clear imaging effect. Therefore, 50 μg mL^{-1} and 15 min were chosen as the best conditions for imaging *Chlorella S.* Subsequently, *Chlorella S.* were co-cultured with R-CDs and commercial lipids dye BODIPY 505/515 to study the distribution of R-CDs. Notably, in order for BODIPY 505/515 to permeate into *Chlorella S.* smoothly, it was necessary to treat *Chlorella S.* with 10% DMSO for 30 min to improve the cell permeability.[50] Colocalization images showed (Fig. $5c_{1-5}$) that the yellow fluorescence of the R-CDs and the green fluorescence of BODIPY 505/515 locations almost overlapped and the Pearson's correlation coefficient was 0.88, which indicated that the R-CDs could specifically target lipids. R-CDs were used to treat two kinds of Chlorella (*Chlorella P.*, *Chlorella S.*) and *Nostoc*. (Fig. 5d). The confocal images of *Chlorella P.* and *Chlorella S.* showed obvious yellow fluorescence, while no fluorescence signal was observed in *Nostoc.*, indicating that *Chlorella* was rich in lipids, while *Nostoc.* had almost no lipids. Studies have shown that *Chlorella* can convert glycolipid into lipid under the condition of nitrogen deficiency.[51] The lipid distribution of *Chlorella S.* grown in BG11 medium and BG11 medium without $NaNO_3$ was compared (Fig. 5e). The chromatophore of *Chlorella S.* with sufficient nutrition occupied a large area, which is beneficial to the photosynthesis of *Chlorella S.*, and the lipids were distributed in the cytoplasm outside the chromatophore. For *Chlorella S.* cultured in N-free BG11, the glycolipid in the body was converted into lipid and the volume of chromatophore was reduced, which indicated the self-protection mechanism of *Chlorella S.* under unfavorable growth conditions.[52,53] The average fluorescence intensity of *Chlorella S.* cultured in N-free BG11 was 1.7 times that of *Chlorella S.* cultured in normal conditions (Fig. 5f), indicating that nitrogen starvation culture could make *Chlorella* produce more lipids, which is consistent with the previously reported results.[54]

Conclusions

In summary, O-PDA was used as a carbon source, and the polarity of the reaction solvent could be adjusted by changing the volume ratio of DMF/H_2O to obtain CDs with different emission wavelengths. The emission center from G-CDs to O-CDs or R-CDs changed from double-emission centers to pure molecular state emission, resulting in the O-CDs and R-CDs being more susceptible to the solvent than the G-CDs. An appropriate polarity of reaction solvent can promote the expansion of π-conjugates of fluorescent molecules on the surface of CDs to realize a red-shift of the emission fluorescence. The red-shift from G-CDs to O-CDs was caused by the expansion of the aromatic structure of fluorescent molecules on the surface of CDs. The slight change from O-CDs to R-CDs was due to the C═O further extending the π-conjugate domain of the whole system. The ICT effect caused by the D–π–A structure of molecules on the surface of R-CDs made them extremely sensitive to the change in solvent polarity and show the characteristics of a high fluorescence intensity in low polarity solvents. Finally, R-CDs were used for the targeted positioning of microalgae lipids, which successfully realized the screening of microalgae lipid-rich varieties and the monitoring of microalgae lipid-content changes under N-free culture conditions.

Author contributions

Fu Fangmei: conceptualization, methodology, formal analysis, writing – original draft preparation, Software, Huang Sirui: formal analysis, writing – reviewing and editing, Pan Xiaoqin: formal analysis, writing – reviewing and editing, Lin Junjie: formal analysis, writing – reviewing and editing, Huang Xiaoman: formal analysis, writing – reviewing and editing, Liang Zishan: formal analysis, writing – reviewing and editing, Zeng Guiling: formal analysis, writing – reviewing and editing, Li Wei: investigation, formal analysis, writing – reviewing and editing, Zhang Haoran: writing – reviewing and editing, Zhang Xuejie: writing – reviewing and editing, Zheng Mingtao: writing – reviewing and editing, Zheng Yinjian: writing – reviewing and editing, Li Qingming: writing – reviewing and editing, Lei Bingfu: supervision, writing – reviewing and editing, project administration, funding acquisition.

Conflicts of interest

There are no conflicts to declare.

Acknowledgements

The work was supported from the Independent Research and Development Projects of Maoming Laboratory (No. 2021ZZ004), the Key Realm R&D Program of Guangdong Province (No. 2021B0707010003), the National Undergraduate Innovation and Entrepreneurship Training Program grant for Sirui Huang (No. 2022), the Guangzhou Science & Technology Project (No. 202007020005, 202103000059), the Project of GDUPS (2018) for Prof. Bingfu LEI, and the Guangdong Provincial Special Fund for Modern Agriculture Industry Technology Innovation Teams (No. 2021KJ122).

Notes and references

1 H. R. Jia, Z. B. Wang, T. Yuan, F. L. Yuan, X. H. Li, Y. C. Li, Z. A. Tan, L. Z. Fan and S. H. Yang, *Adv. Sci.*, 2019, **6**, 1900397.
2 J. J. Liu, Y. J. Geng, D. W. Li, H. Yao, Z. P. Huo, Y. F. Li, K. Zhang, S. J. Zhu, H. T. Wei, W. Q. Xu, J. L. Jiang and B. Yang, *Adv. Mater.*, 2020, **33**(38), 2007162.
3 B. Ju, Y. Wang, Y.-M. Zhang, T. Zhang, Z. H. Liu, M. J. Li and S. X. A. Zhang, *ACS Appl. Mater. Interfaces*, 2018, **10**(15), 13040–13047.
4 H. G. Zhao, G. J. Liu, S. J. You, F. V. A. Camargo, M. Zavelani-Rossi, X. H. Wang, C. C. Sun, B. Liu, Y. M. Zhang, G. T. Han, A. Vomiero and X. Gong, *Energy Environ. Sci.*, 2021, **14**, 396–406.
5 N. K. R. Bogireddy, S. E. S. Rios and V. Agarwal, *Chem. Eng. J.*, 2021, **414**, 128830.
6 X.-Y. Du, C.-F. Wang, G. Wu and S. Chen, *Angew. Chem., Int. Ed.*, 2020, **60**(16), 8585–8595.
7 X. K. Chen, X. D. Zhang, L.-Y. Xia, H.-Y. Wang, Z. Chen and F.-G. Wu, *Nano Lett.*, 2018, **18**(2), 1159–1167.
8 X. C. Sun and Y. Lei, *TrAC, Trends Anal. Chem.*, 2017, **89**, 163–180.
9 Z. F. Wang, F. L. Yuan, X. H. Li, Y. C. Li, H. Z. Zhong, L. Z. Fan and S. H. Yang, *Adv. Mater.*, 2017, **29**(37), 1702910.
10 Y. Y. Jiao, Q. Z. Huang, J. S. Wang, Z. H. He and Z. J. Li, *Appl. Catal., B*, 2019, **247**, 124–132.
11 Y. Q. Zhang, X. Y. Liu, Y. Fan, X. Y. Guo, L. Zhou, Y. Lv and J. Lin, *Nanoscale*, 2016, **8**(33), 15281–15287.
12 D. Li, P. T. Jing, L. H. Sun, Y. An, X. Y. Shan, X. H. Lu, D. Zhou, D. Han, D. Z. Shen, Y. C. Zhai, S. N. Qu, R. Zbořil and A. L. Rogach, *Adv. Mater.*, 2018, **30**(13), 1705913.
13 K. Jiang, S. Sun, L. Zhang, Y. Lu, A. G. Wu, C. Z. Cai and H. W. Lin, *Angew. Chem., Int. Ed.*, 2015, **54**(18), 5360–5363.
14 D. Gao, Y. S. Zhang, A. M. Liu, Y. D. Zhu, S. P. Chen, D. Wei, J. Sun, Z. Z. Guo and H. S. Fan, *Chem. Eng. J.*, 2020, **388**, 124199.
15 D. Gao, A. M. Liu, Y. S. Zhang, Y. D. Zhu, D. Wei, J. Sun, H. R. Luo and H. S. Fan, *Chem. Eng. J.*, 2021, **415**, 128984.
16 Z. J. Zhu, Y. L. Zhai, Z. H. Li, P. Y. Zhu, S. Mao, C. Z. Zhu, D. Du, L. A. Belfiore, J. G. Tang and Y. H. Lin, *Mater. Today*, 2019, **30**, 52–79.
17 H. Ding, J.-S. Wei, P. Zhang, Z.-Y. Zhou, Q.-Y. Gao and H.-M. Xiong, *Small*, 2018, **14**, 1800612.
18 C. J. Burrows, J. B. Harper, W. Sander and D. J. Tantillo, *J. Org. Chem.*, 2022, **87**(3), 1599–1601.
19 P. D. Khavlyuk, E. A. Stepanidenko, D. P. Bondarenko, D. V. Danilov, A. V. Koroleva, A. V. Baranov, V. G. Maslov, P. Kasak, A. V. Fedorov, E. V. Ushakova and A. L. Rogach, *Nanoscale*, 2021, **13**(5), 3070–3078.
20 S. J. Zhu, Y. B. Song, X. H. Zhao, J. R. Shao, J. H. Zhang and B. Yang, *Nano Res.*, 2022, **8**, 355–381.
21 L. Wang, W. T. Li, L. Q. Yin, Y. J. Liu, H. Z. Guo, J. W. Lai, Y. Han, G. Li, M. Li, J. H. Zhang, R. Vajtai, P. M. Ajayan and M. H. Wu, *Sci. Adv.*, 2020, **6**, eabb6772.
22 S. R. Medipally, F. M. Yusoff, S. Banerjee and M. Shariff, *Biomed Res. Int.*, 2015, **14**(1), 217–232.
23 H. D. Siegler, W. Ayidzoe, A. Ben-Zvi, R. E. Burrell and W. C. Mccaffrey, *Algal Res.*, 2012, **1**(2), 176–184.
24 W. Chen, C. W. Zhang, L. R. Song, M. Sommerfeld and Q. Hu, *J. Microbiol. Methods*, 2009, **77**(1), 41–47.
25 J. Rumin, H. Bonnefond, B. Saint-Jean, C. Rouxel, A. Sciandra, O. Bernard, J. P. Cadoret and G. Bougaran, *Biotechnol. Biofuels*, 2015, **8**, 42.
26 C. She, Z. H. Wang, J. Zeng and F. G. Wu, *Carbon*, 2022, **191**, 636–645.
27 C. Sudfeld, M. Hubaek, S. Adamo, R. H. Wijffels and M. J. Barbosa, *Algal Res.*, 2020, **53**, 102138.
28 X. K. Xu, L. Q. Mo, Y. D. Li, X. Q. Pan, G. Q. Hu, B. F. Lei, X. J. Zhang, M. T. Zheng, J. L. Zhuang, Y. L. Liu and C. F. Hu, *Adv. Mater.*, 2021, **33**(49), 2104872.
29 X. Q. Lin and H. Q. Zhang, *Electrochim. Acta*, 1996, **41**(13), 2019–2024.
30 I. M. Khan and A. Ahmad, *Spectrochim. Acta, Part A*, 2010, **76**(3–4), 315–321.
31 S. Y. Tang, D. Chen, Y. S. Yang, C. X. Wang, X. M. Li, Y. R. Wang, C. J. Gu and Z. Cao, *J. Colloid Interface Sci.*, 2022, **617**, 182–192.
32 F. L. Yuan, T. Yuan, L. Z. Sui, Z. B. Wang, Z. F. Xi, Y. C. Li, X. H. Li, L. Z. Fan, Z. A. Tan, A. M. Chen, M. X. Jin and S. H. Yang, *Nat. Commun.*, 2018, **9**, 2249.
33 M. Fu, X. C. Ji, Y. T. Li, G.-J. Deng and H. W. Huang, *Green Chem.*, 2020, **22**(17), 5594–5598.
34 Q. Zhang, R. Y. Wang, B. W. Feng, X. X. Zhong and K. Ostrikov, *Nat. Commun.*, 2021, **12**(1), 6856.
35 M.-X. Liu, N. Ding, S. Chen, Y. L. Yu and J.-H. Wang, *Anal. Chem.*, 2021, **93**, 5284–5290.
36 L. Cao, M. H. Zan, F. M. Chen, X. Y. Kou, Y. L. Liu, P. Y. Wang, Q. Mei, Z. Hou, W.-F. Dong and L. Li, *Carbon*, 2022, **194**, 42–51.
37 N. Jiang, J. L. Fan, F. Xu, X. J. Peng, H. Y. Mu, J. Y. Wang and X. Q. Xiong, *Angew. Chem., Int. Ed.*, 2015, **54**(8), 2510–2514.
38 K. N. Wang, S. Y. Ma, Y. Y. Ma, Y. P. Zhao, M. M. Xing, L. Y. Zhou, D. X. Cao and W. Y. Lin, *Anal. Chem.*, 2020, **92**(9), 6631–6636.
39 Z.-E. Chen, Q.-L. Qi and H. Zhang, *Spectrochim. Acta, Part A*, 2020, **238**, 118384.
40 J. H. Liu, D. Y. Li, J. H. He, D. Yuan, R. S. Li, S. J. Zhen, Y. F. Li and C. Z. Huang, *ACS Appl. Mater. Interfaces*, 2020, **12**(4), 4815–4820.

41 Y. Q. Dong, H. C. Pang, H. B. Yang, C. X. Guo, J. W. Shao, Y. W. Chi, C. M. Li and T. Yu, *Angew. Chem., Int. Ed.*, 2013, **52**(30), 7800–7804.
42 L. Wang, S.-J. Zhu, H.-Y. Wang, S.-N. Qu, Y.-L. Zhang, J.-H. Zhang, Q.-D. Chen, H.-L. Xu, W. Han, B. Yang and H.-B. Sun, *ACS Nano*, 2014, **8**(3), 2541–2547.
43 B. Y. Wang, J. K. Yu, L. Z. Sui, S. J. Zhu, Z. Y. Tang, B. Yang and S. Y. Lu, *Adv. Sci.*, 2020, **8**(1), 2001453.
44 T. X. Zhang, J. Y. Zhu, Y. Zhai, H. Wang, X. Bai, B. Dong, H. Y. Wang and H. W. Song, *Nanoscale*, 2017, **9**(35), 13042–13051.
45 Y. J. Zhang, R. R. Yuan, M. L. He, G. C. Hu, J. T. Jiang, T. Xu, L. Zhou, W. Chen, W. D. Xiang and X. J. Liang, *Nanoscale*, 2017, **9**(45), 17849–17858.
46 L. Wang, S.-J. Zhu, H.-Y. Wang, Y.-F. Wang, Y.-W. Hao, J.-H. Zhang, Q.-D. Chen, Y.-L. Zhang, W. Han, B. Yang and H.-B. Sun, *Adv. Opt. Mater.*, 2013, **1**(3), 264–271.
47 C. Qiang, B. Luigi, D. Lakshya, K. S. Mali, F. S. De, T. Matteo, M. Klaus and N. Akimitsu, *Angew. Chem., Int. Ed.*, 2018, **57**, 11233–11237.
48 G. Albano, T. Colli, L. Nucci, R. Charaf, T. Biver, A. Pucci and L. A. Aronica, *Dyes Pigm.*, 2020, **174**, 108100.
49 S. Kotha, R. Ali, N. R. Panguluri, A. Datta and K. K. Kannaujiya, *Tetrahedron Lett.*, 2018, **59**, 4080–4085.
50 H. A. Aratboni, N. Rafiei, R. Garcia-Granados., A. Alemzadeh and J. R. Morones-Ramírez, *Microb. Cell Fact.*, 2019, **18**, 178.
51 W. Chen, M. Sommerfeld and Q. Hu, *Bioresour. Technol.*, 2011, **102**, 135–141.
52 Y. L. Jiang, T. Yoshida and A. Quigg, *Plant Physiol. Biochem.*, 2012, **54**, 70–77.
53 N. Shtaida, I. Khozin-Goldberg, A. Solovchenko, K. Chekanov, S. Didi-Cohen, S. Leu, Z. Cohen and S. Boussiba, *J. Exp. Bot.*, 2014, **65**, 6563–6576.
54 R. Rengel, R. T. Smith, R. P. Haslam, O. Sayanova, M. Vila and R. León, *Algal Res.*, 2018, **31**, 183–193.